Spatial Green Function of a Constant Medium Overlying a Duct With Linear-Square Refractive Index Profile

Christophe Bourlier and Nicolas Pinel

***Abstract*—For a two-dimensional problem, this paper presents the evaluation of the spatial Green function of environments made up of a constant medium overlying a duct having a linear-square refractive index profile. This function must be determined to deal with the more general problem of scattering from a rough sea surface in the presence of a duct. Indeed, knowing the spatial Green function, the sea surface roughness effect can be taken into account rigorously in the calculation of the scattered field by solving the integral equations on the rough surface. Assuming a slowly-varying refractive index profile, by using the method of steepest descents, closed-form expressions of the spatial Green function in different regions (illuminated and shadowed) are derived. In addition, they are compared with that obtained from the parabolic wave equation.**

***Index Terms*—Ducting environments, Green function, inhomogeneous media, parabolic wave equation, saddle point technique.**

I. Introduction

In the past decades, researchers in the areas of applied electromagnetics and underwater acoustics developed rigorous and asymptotic models for mathematically describing the wave propagation over rough surfaces as well as the scattering of these waves by such surfaces. These studies also investigated the combined effects of atmospheric conditions (ducting conditions) and surface roughness on the propagation and scattering problem. To solve this issue, two main methods are available in the literature: the well-known parabolic wave equation (PWE) method [1] and the boundary integral equation (BIE) method [2]–[4].

Under the conditions of predominant forward propagation and scattering, i.e., when the rough surface is gently undulating and the angles of propagation and scattering are grazing, the PWE approximation gives satisfactory results. For a complete review of this method, see the textbook of M. Levy [1] and the references therein. The great advantage of the PWE method is that it can deal with most real-life inhomogeneous environments. Its main drawback is the underlying paraxial approximation leading to an approximation of the propagator (that is, the Green function).

By contrast, the BIE method, which is based on the Helmholtz wave equation, rigorously calculates all the surface field interactions. If the Green function is known in an appropriate (spatial or spectral) domain, an integral equation can be written for the induced currents on a rough surface. These currents are then used in radiation integrals involving the appropriate propagators to calculate the scattered field at a point above the surface. The advantage of the BIE method is that it is a rigorous method, but its main drawback is that the Green function (propagator) is known only for a small class of refractive index profiles [5], [6]. That is why, when the BIE method is applied [2], the propagator is usually derived under the PWE approximation.

More recently, for an half-space having a linear square refractive index profile ($n^2(z) = 1 - \varepsilon z$, with $0 < \varepsilon \ll 1$ and the height $z \geq 0$, meaning that the transmitter and receiver heights check $z_{\mathrm{T}} \geq 0$ and $z_{\mathrm{R}} \geq 0$, respectively), Awadallah and Brown [3], [4] derived a more rigorous Green function used to calculate the currents on a perfectly-conducting rough surface from the BIE method. For this specific case and in the spectral domain, the exact Green function is expressed in terms of Airy functions. But, in the spatial domain, its inverse Fourier transform is not numerically tractable, since the involved integrals are difficult to evaluate even numerically, due to the oscillatory nature of the integrands. Consequently, an approximate solution, which is valid in the frequency range of interest (i.e., the microwave range), is obtained asymptotically by using the method of SD (Steepest Descents) [3], [6], [7] combined with the WKB (Wentzel-Kramers-Brillouin) [6] approximation. The latter is valid for a slowly-varying refractive index profile. Then, the method presented in [3] allows us to validate algorithms based on the PWE. For practical applications, the condition $z_{\mathrm{T}} \geq 0$ and $z_{\mathrm{R}} \geq 0$ is not met because it corresponds to an environment having a refractive index n lower than one, since $n^2(z) = 1 - \varepsilon z$ with $\varepsilon > 0$.

In many physical ducting environments, the refractive index profile decreases with increasing height up to a given altitude, and eventually reaches a constant value. The purpose of this paper is to derive the spatial Green function of such environments by using the method presented in [8], [9]. It is important to note that in the case $z \leq 0$, the derivation of the spatial Green function strongly differs from the case $z \geq 0$ (presented in [3], [4] for the special case of a space having a linear square refractive index profile for all z). In addition, this function is compared with that obtained under the PWE.

Manuscript received October 22, 2012; revised January 25, 2013; accepted February 11, 2013. Date of publication March 19, 2013; date of current version May 29, 2013.

The authors are with IETR (Institut d'Electronique et de Télécommunications de Rennes) Laboratory, LUNAM Université, Université de Nantes, Polytech Nantes, 44306 Nantes Cedex 3, France (e-mail: christophe.bourlier@univ-nantes.fr).

Color versions of one or more of the figures in this paper are available online at http://ieeexplore.ieee.org.

Digital Object Identifier 10.1109/TAP.2013.2253300

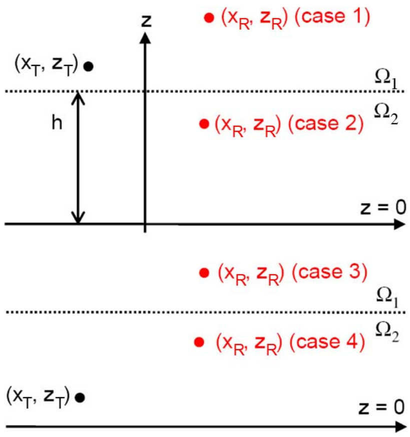

Fig. 1. Illustration of the different cases for the calculation of the Green function, with $(x_{\rm T}, z_{\rm T})$ the coordinates of the transmitter and $(x_{\rm R}, z_{\rm R})$ those of the receiver. Case 1: $z_{\rm T} \geq h$ and $z_{\rm R} \geq h$. Case 2: $z_{\rm T} \geq h$ and $z_{\rm R} < h$. Case 3: $z_{\rm T} < h$ and $z_{\rm R} \geq h$. Case 4: $z_{\rm T} < h$ and $z_{\rm R} < h$.

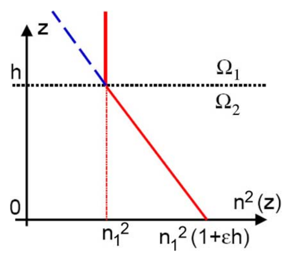

Fig. 2. Profile of the square refractive index $n^2(z)$.

Section II presents the spectral Green function for a homogeneous medium overlying a duct with linear-square refractive index profile, whereas in Section III, an evaluation of the corresponding spatial Green function is addressed. Moreover, Section III presents numerical results and a comparison with the PWE. The last section gives concluding remarks.

II. Spectral Green Function

Let us consider a two-dimensional space $\Omega = \Omega_1 \cup \Omega_2$ (see Figs. 1 and 2) made up of a homogeneous medium Ω_1 (defined for $z \geq h$) of constant refractive index n_1 over an inhomogeneous one Ω_2 (defined for $z < h$, duct), with a linear-square refractive index profile defined by $n^2(z) = n_1^2 - \varepsilon'(z-h)$, with $\varepsilon' > 0$. $h > 0$ denotes the duct height. Inside Ω_2, for $z = 0$, $n^2(0) = n_1^2 + \varepsilon' h > n_1^2$ (since $\varepsilon' > 0$ and $h > 0$) and $n(h) = n_1$. We define in Ω_1 the wavenumber $k_1 = k_0 n_1$, where k_0 is the wavenumber in free space. In addition, $\varepsilon = \varepsilon'/n_1^2$ such that in Ω_2, $n^2(z) = n_1^2[1 - \varepsilon(z-h)]$. Thus, in Ω_2, the refractive index is $n(z) = n_1\sqrt{1-\varepsilon(z-h)} = \sqrt{1+\varepsilon(h-z)}$.

Awadallah and Brown [3], [4] assumed that $n^2(z') = n_1^2 - \varepsilon z', \forall z'$ $(n_1 = 1)$ and studied the special case $z' \geq 0$. It is then equivalent to consider the case $z' = z - h \geq 0 \Leftrightarrow z \geq h$, for which the transmitter and the receiver are in Ω_1 of refractive index shows in dashed straight line in Fig. 2. For practical applications, the transmitter can be located inside the duct, for which the refractive index is greater than one. It is then relevant to study this case.

A. General Case

In this section, we consider the general case: the source (transmitter) can be either in medium Ω_i $(i = \{1,2\})$ or in medium Ω_j $(j = \{1,2\} \neq i)$ or a source can be located on each medium. In addition, $z_{\rm T}$ and $z_{\rm R}$ are the transmitter and receiver heights, respectively.

In Ω_i, the spectral Green function can be written as

$$\hat{g}_i = \hat{u}_i + A_i \hat{v}_i \tag{1}$$

where the functions $\hat{u}_i$ and $\hat{v}_i$ depend on $(k_{1x} = k_1 \sin\theta, z_{\rm R}, z_{\rm T})$, whereas A_i depends on $(k_{1x}, h, z_{\rm T})$. The term A_i can be physically interpreted as a reflection or transmission coefficient and it will be computed from the boundary conditions applied at $z = h$. In the spectral domain, the two independent functions $\hat{f} = \{\hat{u}_i, \hat{v}_i\}$ (eigen functions) satisfy the propagation equation $\partial_z^2 \hat{f} + [k_1^2 n^2(z) - k_{1x}^2]\hat{f} = 0$, where $\partial_z^2 = \partial^2/\partial z^2$. The function $\hat{u}_i$ is a downgoing wave coming from $z = +\infty$ whereas $\hat{v}_i$ is an upgoing wave coming from $z = -\infty$.

To determine A_i, the boundary conditions at the interface $z = h$ are applied. Assuming that $n(h_+) = n(h_-)$ (continuity of the refractive index at $z = h$), they state $\forall z_{\rm T}$ and at $z = h$ that

$$\hat{g}_1 = \hat{g}_2, \quad \partial_z \hat{g}_1 = \partial_z \hat{g}_2. \tag{2}$$

Thus, for $z = h$, we obtain

$$\begin{cases} A_1 = \left.\frac{w_{21} - w_{11}}{\hat{v}_1 \partial_z \hat{v}_2 - \hat{v}_2 \partial_z \hat{v}_1}\right|_{z=h} \\ A_2 = \left.\frac{w_{11} - w_{12}}{\hat{v}_1 \partial_z \hat{v}_2 - \hat{v}_2 \partial_z \hat{v}_1}\right|_{z=h} \end{cases} \tag{3}$$

where the Wronskian w_{ij} is defined as

$$w_{ij} = \hat{v}_i \partial_z \hat{u}_j - \hat{u}_i \partial_z \hat{v}_j \tag{4}$$

in which $\partial_z = \partial/\partial z$.

B. Cases 1 and 2: Transmitter Outside the duct ($z_{\rm T} \geq h$)

For $z_{\rm T} \geq h$ (cases 1 or 2 in Fig. 1, corresponding to the transmitter outside the duct), in the spectral domain, the functions u_i and v_i are expressed as [6], [8]

$$\begin{cases} \hat{u}_1(k_{1x}; z_{\rm R}, z_{\rm T}) = \frac{j e^{jk_{1z}|z_{\rm T} - z_{\rm R}|}}{2k_{1z}} \\ \hat{v}_1(k_{1x}; z_{\rm R}, z_{\rm T}) = \frac{j e^{jk_{1z}(z_{\rm T} + z_{\rm R})}}{2k_{1z}} \\ \hat{u}_2(k_{1x}; z_{\rm R}, z_{\rm T}) = 0 \\ \hat{v}_2(k_{1x}; z_{\rm R}, z_{\rm T}) = w_1(k_{1x}; z_{\rm R}) = w_1(t_{\rm R}) \end{cases} \tag{5}$$

in which $t_{\rm R}$ is expressed as

$$\begin{cases} t_{\rm R} = t + \frac{z_{\rm R} - h}{H}, \quad H = \frac{1}{(\varepsilon k_1^2)^{\frac{1}{3}}} \\ t = H^2\left(k_{1x}^2 - k_1^2\right) = -H^2 k_{1z}^2 = -\left(\frac{k_1}{\varepsilon}\right)^{\frac{2}{3}} \cos^2\theta \end{cases}. \tag{6}$$

It can be noted that $k_{1z} = k_1 \cos\theta$, and $\hat{u}_2 = 0$ because there is no source in medium Ω_2 as $z_{\rm T} \geq h$. In addition, $\hat{v}_2(t) = w_1(t) = u(t) + jv(t)$ satisfies $\hat{v}_2(-\infty) = 0$. The functions u and v are defined as $v(t) = \sqrt{\pi}\mathrm{Ai}(t)$ and $u(t) = \sqrt{\pi}\mathrm{Bi}(t)$, in which Ai and Bi are the Airy functions.

From (3), the reflection $\mathcal{R} = A_1$ and transmission $\mathcal{T} = A_2$ coefficients at the interface between Ω_1 and Ω_2 are given by

$$\begin{cases} \mathcal{R} = \frac{1-\alpha}{1+\alpha} e^{-j2k_{1z}h} \\ \mathcal{T} = \frac{je^{jk_{1z}(z_{\mathrm{T}}-h)}}{k_{1z}w_1(t)(1+\alpha)} \end{cases} \tag{7}$$

with

$$\alpha = \frac{jw_1'(t)}{\sqrt{-t}w_1(t)} \tag{8}$$

and $\partial_{z_{\mathrm{R}}} t_{\mathrm{R}} = 1/H$ from (6).

For $z_{\mathrm{T}} \geq h$, from (5) and (7), the total Green function is then

$$\hat{g}(k_{1x}; z_{\mathrm{R}}, z_{\mathrm{T}}) = \begin{cases} \frac{j}{2k_{1z}} \Big[e^{jk_{1z}|z_{\mathrm{T}}-z_{\mathrm{R}}|} \\ \quad + \frac{1-\alpha}{1+\alpha} e^{jk_{1z}(z_{\mathrm{T}}+z_{\mathrm{R}}-2h)} \Big] & z_{\mathrm{R}} \geq h \\ \frac{jw_1(t_{\mathrm{R}})e^{jk_{1z}(z_{\mathrm{T}}-h)}}{k_{1z}w_1(t)(1+\alpha)} & z_{\mathrm{R}} < h \end{cases}. \tag{9}$$

For $z_{\mathrm{R}} \geq h$, it can be noted that the term $2h - z_{\mathrm{T}}$ inside the second exponential function equals the height of the transmitter image with respect to $z = h$.

C. Cases 3 and 4: Transmitter Inside the Duct Ω_2 ($z_{\mathrm{T}} < h$)

For $z_{\mathrm{T}} < h$ (cases 3 or 4 in Fig. 1, corresponding to the transmitter inside the duct), in the spectral domain, the functions u_i and v_i are expressed as [6], [8]

$$\begin{cases} \hat{u}_1(k_{1x}; z_{\mathrm{R}}, z_{\mathrm{T}}) = 0 \\ \hat{v}_1(k_{1x}; z_{\mathrm{R}}, z_{\mathrm{T}}) = \frac{je^{jk_{1z}z_{\mathrm{R}}}}{2k_{1z}} \\ \hat{u}_2(k_{1x}; z_{\mathrm{R}}, z_{\mathrm{T}}) = Hw_1(t_-)v(t_+) \\ \hat{v}_2(k_{1x}; z_{\mathrm{R}}, z_{\mathrm{T}}) = Hw_1(t_-)w_1(t_+) \end{cases} \tag{10}$$

in which $t_+ = \max(t_{\mathrm{T}}, t_{\mathrm{R}})$, $t_- = \min(t_{\mathrm{T}}, t_{\mathrm{R}})$ and t_{T} has the same expression as t_{R} except z_{T} replaces z_{R}. It can be noted that $\hat{u}_1 = 0$ because there is no source in medium Ω_1 as $z_{\mathrm{T}} < h$.

From (3), the reflection $\mathcal{R} = A_2$ and transmission $\mathcal{T} = A_1$ coefficients at the interface between Ω_2 and Ω_1 are given by

$$\begin{cases} \mathcal{R} = -\frac{v'(t)-jv(t)\sqrt{-t}}{w_1'(t)-jw_1(t)\sqrt{-t}} \\ \mathcal{T} = \frac{2e^{-jk_{1z}h}w_1(t_{\mathrm{T}})}{w_1(t)(1+\alpha)} \end{cases} \tag{11}$$

where $w_1'(t)v(t) - w_1(t)v'(t) = 1$ since the Wronskrian $u'(t)v(t) - u(t)v'(t) = 1$.

For $z_{\mathrm{T}} < h$, from (10) and (11), the total Green function is then

$$\hat{g}(k_{1x}; z_{\mathrm{R}}, z_{\mathrm{T}}) = \begin{cases} \frac{jw_1(t_{\mathrm{T}})e^{jk_{1z}(z_{\mathrm{R}}-h)}}{k_{1z}w_1(t)(1+\alpha)} & z_{\mathrm{R}} \geq h \\ Hw_1(t_-)\Big[v(t_+) \\ \quad - \frac{v'(t)-jv(t)\sqrt{-t}}{w_1'(t)-jw_1(t)\sqrt{-t}} w_1(t_+)\Big] & z_{\mathrm{R}} < h \end{cases}. \tag{12}$$

For $z_{\mathrm{R}} \geq h$, (12) is the same as (9) obtained for $z_{\mathrm{R}} < h$ by substituting z_{R} for z_{T}, which is in agreement with the reciprocity principle.

III. Evaluation of the Spatial Green Function

A. Definition

The 2D spatial Green function can be defined from the 2D spectral Green function as

$$g(X; z_{\mathrm{R}}, z_{\mathrm{T}}) = \frac{1}{2\pi} \int_{-\infty}^{+\infty} \hat{g}(k_{1x}; z_{\mathrm{R}}, z_{\mathrm{T}}) e^{jk_{1x}X} dk_{1x} \tag{13}$$

where $\hat{g}(k_{1x}; z_{\mathrm{R}}, z_{\mathrm{T}})$ is the spectral Green function derived in the previous section. In addition, $X = x_{\mathrm{R}} - x_{\mathrm{T}}$ equals the abscissa difference between the receiver and the transmitter.

The inverse Fourier transform (13) is not numerically tractable, since the involved integral is difficult to evaluate even numerically, due to the strongly oscillatory nature of the integrand in the frequency range of interest (high frequencies). Consequently, an approximate solution, which is valid in the frequency range of interest (i.e., the microwave range), is obtained asymptotically by using the method of SD (steepest descents).

For an half-space having a linear square refractive index profile ($n^2(z) = 1 - \varepsilon z$, with $0 < \varepsilon \ll 1$ and the height $z \geq 0$, meaning that the transmitter and receiver heights satisfy $z_{\mathrm{T}} \geq 0$ and $z_{\mathrm{R}} \geq 0$, respectively), Awadallah and Brown [3], [4] derived (13) by using the method of SD (Steepest Descents) [6], [7] combined with the WKB (Wentzel-Kramers-Brillouin) [6] approximation. The latter is valid for a slowly-varying refractive index profile. Moreover, for practical applications, the case $z_{\mathrm{T}} \geq 0$ and $z_{\mathrm{R}} \geq 0$ is not met because it corresponds to a refractive index lower than one since $n^2(z) = 1 - \varepsilon z$ with $\varepsilon > 0$. It is important to note that for the case $n^2(z) \geq 1$, the derivation of the spatial Green function strongly differs from the case $n^2(z) \leq 1$ (presented in [3], [4] for the special case of a space having a linear square refractive index profile for all z).

Then, in this paper, an approximate solution of (13) is obtained from the works published by Fock [8] and Kukushkin [9].

B. Green Function for $z_{\mathrm{T}} < h$: Transmitter Inside the Duct

1) Green Function for $z_R < h$: Receiver Inside the Duct: For $z_{\mathrm{R}} < h$ (case 4 of Fig. 1), the spectral Green function is expressed from (12). From (6), $\{t, t_{\mathrm{R}}, t_{\mathrm{T}}\}$ are real. In (12), this implies that the functions v and u take real values and then, $w_1^* = u - jv = w_2$ since $w_1 = u + jv$. Equation (12) is then expressed from $\{w_1, w_2\}$ as

$$\hat{g}(k_{1x}; z_{\mathrm{R}}, z_{\mathrm{T}}) = \frac{jHw_1(t-\nu_-)}{2} \Big[w_2(t-\nu_+) \\ - \frac{w_2'(t) - q(t)w_2(t)}{w_1'(t) - q(t)w_1(t)} w_1(t-\nu_+) \Big] \tag{14}$$

where $\nu_+ = [h - \min(z_{\mathrm{R}}, z_{\mathrm{T}})]/H \geq 0$, $\nu_- = [h - \max(z_{\mathrm{R}}, z_{\mathrm{T}})]/H \geq 0$ and $q(t) = j\sqrt{-t} = j(k_1/\varepsilon)^{1/3}\cos\theta$. The spectral Green function [8] (chapter 12) is then the same as that of a dipole above a circular highly-conducting surface of radius r_0, which is much greater than the wavelength λ_1 ($k_1 r_0 \gg 1$). In this case, $q = j(k_1 r_0/2)^{1/3}/n_0$, in which n_0 is the refractive index of the surface, which is a **constant**. Thus, the duct problem is equivalent to take this case by taking

$\cos\theta = 1/n_0$ and $\varepsilon = 2/r_0 \ll 1$. For a highly-conducting surface, the refractive index modulus $|n_0| \gg 1$, which corresponds to $|\cos\theta| \to 0$. Here, it is important to note that q depends on t whereas in [8], q is a constant.

With the PWE, the Green function is expressed as [2]

$$g_{\text{PWE}} = \begin{cases} \frac{je^{-j\pi/4}}{2\sqrt{2\pi k_1 X}} e^{jk_1\left(R+\frac{\varepsilon(2h-z_{\text{R}}-z_{\text{T}})X}{4}-\frac{\varepsilon^2 X^3}{96}\right)} & \text{if } X \geq 0 \\ 0 & \text{otherwise} \end{cases} \quad (15)$$

In addition, with the PWE, the radial distance $R = \sqrt{X^2 + (z_{\text{R}} - z_{\text{T}})^2}$ between the transmitter and the receiver can be approximated in the phase term as $R \approx X + (z_{\text{R}} - z_{\text{T}})^2/(2X)$, whereas in the amplitude term $R \approx X$.

To calculate the spatial Green function, the inverse Fourier transform (see (13)) of $\hat{g}(k_{1x}; z_{\text{R}}, z_{\text{T}})$ must be derived. An evaluation of this kind of integral is reported in the textbook of [8] (chapter 7) and [9] (appendix A), in which the saddle points are assumed to be close to $\pi/2$. The integral over k_{1x} ((13)) can then be converted into an integral over t, knowing that θ is close to $\pi/2$. We have then,

$$\begin{aligned} t &= -H^2 k_1^2 \cos^2\theta = -H^2 k_1^2 (1 - \sin\theta)(1 + \sin\theta) \\ &\approx -2H^2 k_1^2 (1 - \sin\theta). \end{aligned} \quad (16)$$

In addition, from (16), $dt \approx 2H^2 k_1^2 d(\sin\theta) = 2H^2 k_1 dk_{1x}$ since $k_{1x} = k_1 \sin\theta$. The substitution of (16) and (14) into (13) leads then to

$$g(X; z_{\text{R}}, z_{\text{T}}) \approx g_D(X; z_{\text{R}}, z_{\text{T}}) - g_R(X; z_{\text{R}}, z_{\text{T}}) \quad (17)$$

where

$$g_D(X; z_{\text{R}}, z_{\text{T}}) \approx \frac{je^{jk_1X}}{8\pi H k_1} \int_C w_1(t - \nu_-) w_2(t - \nu_+) e^{j\xi t} dt \quad (18)$$

$$g_R(X; z_{\text{R}}, z_{\text{T}}) \approx \frac{je^{jk_1X}}{8\pi H k_1} \int_C \left[w_1(t - \nu_-) w_1(t - \nu_+) - \frac{w_2'(t) - j\sqrt{-t}\, w_2(t)}{w_1'(t) - j\sqrt{-t}\, w_1(t)} \right] e^{j\xi t} dt \quad (19)$$

and $\xi = X/(2H^2 k_1)$. In (18) and (19), the subscripts "D" and "R" refer to direct and reflected (Green function), respectively. The contour C in integrals (18) and (19) encloses in the positive direction the first quadrant of the complex t plane (all the poles of the integrand are located in this quadrant). In the following, from (13), since $g(-X; z_{\text{R}}, z_{\text{T}}) = g(X; z_{\text{R}}, z_{\text{T}})$, we have $g(-\xi; z_{\text{R}}, z_{\text{T}}) = g(\xi; z_{\text{R}}, z_{\text{T}})$ and then, only the case $\xi \geq 0$ is considered.

The problem solved in [11], [12] is different of ours. In these references, a boundary is added corresponding to the Earth assumed to be highly-conducting. Then, the resulting Green function is expressed as Eq. (19) of [11], in which the denominator of the integrand has zeros (or poles for the integrand). Then, the spatial Green function is expressed as an infinite sum of combined Airy functions (normal mode expansion), in which roots must be determined. Here, this method can not be applied, because in (19) the reflection coefficient has no pole (because no boundary; in other words, no bounce on the Earth from a ray approach).

To find an approximate solution of integrals (18) and (19), two regions are considered: the illuminated and shadow regions.

a) Illuminated region: Mathematically, this region corresponds to $t \ll 0$ and $t - \nu_\pm \ll 0$, which is equivalent to apply the WKB approximation. Then, from (A1) and (A2), we have

$$\begin{cases} w_1(t - \nu_-) \approx e^{+j\pi/4} (\nu_- - t)^{-1/4} e^{+\frac{2j}{3}(\nu_- - t)^{\frac{3}{2}}} \\ w_2(t - \nu_+) \approx e^{-j\pi/4} (\nu_+ - t)^{-1/4} e^{-\frac{2j}{3}(\nu_+ - t)^{\frac{3}{2}}} \\ \mathcal{R} = \frac{w_2'(t) - j\sqrt{-t}\, w_2(t)}{w_1'(t) - j\sqrt{-t}\, w_1(t)} \approx \frac{1}{8(-t)^{\frac{3}{2}}} e^{-\frac{4j(-t)^{\frac{3}{2}}}{3}} \end{cases} . \quad (20)$$

To approximate $\mathcal{R}$, (A1) and (A2) are applied up to the first order (the terms along a_1 and b_1 are kept). As $|t|$ increases, $|\mathcal{R}|$ decreases.

The substitution of (20) into (18) and (19) leads to

$$g_D(X; z_{\text{R}}, z_{\text{T}}) \approx \frac{je^{jk_1X}}{8\pi H k_1} \int_C \frac{e^{j\phi_D(t)} dt}{[(\nu_+ - t)(\nu_- - t)]^{\frac{1}{4}}} \quad (21)$$

$$g_R(X; z_{\text{R}}, z_{\text{T}}) \approx \frac{je^{jk_1X}}{8\pi H k_1} \int_C \frac{e^{j\phi_R(t)} dt}{8\left[(\nu_+ - t)(\nu_- - t)\right]^{\frac{1}{4}} (-t)^{\frac{3}{2}}} \quad (22)$$

where

$$\begin{cases} \phi_D(t) = \xi t + \frac{2}{3}(\nu_- - t)^{\frac{3}{2}} - \frac{2}{3}(\nu_+ - t)^{\frac{3}{2}} \\ \phi_R(t) = \xi t + \frac{2}{3}(\nu_- - t)^{\frac{3}{2}} + \frac{2}{3}(\nu_+ - t)^{\frac{3}{2}} - \frac{4}{3}(-t)^{\frac{3}{2}} \end{cases} . \quad (23)$$

If a function $f(t)$ has no singularities near a (single) saddle point t_s of a real function $\phi(t)$, where $\phi'(t_s) = 0$ and $\phi''(t_s) \neq 0$, for $|\phi| \gg 1$, then ([7], chapter 4, page 382)

$$\int_{-\infty}^{+\infty} f(t) e^{i\phi(t)} dt \approx \sqrt{\frac{2\pi}{|\phi''(t_s)|}} f(t_s) e^{j\phi(t_s) + j\text{sgn}\left(\phi''(t_s)\right)\pi/4} \quad (24)$$

in which the symbol sgn denotes the sign function.

For the function ϕ_D, we have $\phi_D' = \xi - \sqrt{\nu_- - t} + \sqrt{\nu_+ - t}$. The saddle point is then $t_s = -\xi^2/4 + (\nu_+ + \nu_-)/2 - (\nu_+ - \nu_-)/(4\xi^2)$. In addition, $\phi_D''(t_s) = 1/(2\sqrt{\nu_- - t_s}) - 1/(2\sqrt{\nu_+ - t_s}) = -\xi/[2\sqrt{\nu_- - t_s}\sqrt{\nu_+ - t_s}] < 0$. Then, using (24) and from (21), we obtain

$$g_D(X; z_{\text{R}}, z_{\text{T}}) \approx \frac{je^{-j\pi/4 + jk_1X}}{2\sqrt{2\pi k_1 X}} \times e^{j\phi_D(t_s)} \quad (25)$$

where

$$\phi_D(t_s) = -\frac{\varepsilon^2 X^3 k_1}{96} + \frac{\varepsilon X(2h - z_{\text{R}} - z_{\text{T}})k_1}{4} + \frac{(z_{\text{R}} - z_{\text{T}})^2 k_1}{2X}. \quad (26)$$

With the PWE, the Green function is expressed from (15). The comparison of (15) with (25) leads then to $g_{\text{PWE}} = g_D$.

Using the same way for the evaluation of integral (22), we show in Appendix C that

$$g_R(X; z_{\text{R}}, z_{\text{T}}) \approx \frac{je^{-j\pi/4 + jk_1X + j\phi_R(s_0)}}{16 p_0^3 \sqrt{2\pi k_1 X}} \times \sqrt{\frac{\xi}{2}} \sqrt{\frac{2(\nu_+ - \nu_- + \xi s_0)}{(\nu_+ - \nu_-)\xi + s_0^3}} \quad (27)$$

where s_0, p_0 and $\phi_R(s_0)$ are expressed from (C5), (C6) and (C7), respectively. To give a physical explanation of (27), the case

$$\xi^2 \ll 2(\nu_+ + \nu_-) \Rightarrow X \ll 2\sqrt{\frac{2(2h - z_\mathrm{T} - z_\mathrm{R})}{\varepsilon}} = X_1 \quad (28)$$

is considered. For example, for $h = 20$ m, $z_\mathrm{T} = 10$ m, $z_\mathrm{R} = 0$ and $\varepsilon = 0.0001\ \mathrm{m}^{-1}$, we have $X_1 \approx 1549$ m. For this case:

$$\begin{cases} s_0 \approx \frac{2\mu\alpha}{3} \approx \frac{2\sqrt{2}\sqrt{\nu_+ + \nu_-}}{\sqrt{3}} \\ \phi_R(s_0) - \phi_D(t_s) \approx \frac{\nu_+ \nu_-}{\xi} \\ \sqrt{\frac{\xi}{2}}\sqrt{\frac{2(\nu_+ - \nu_- + \xi s_0)}{(\nu_+ - \nu_-)\xi + s_0^3}} \approx 1 \end{cases}. \quad (29)$$

Reporting (29) into (27) and using (25), the total spatial Green function is

$$g_D(X; z_\mathrm{R}, z_\mathrm{T}) - g_R(X; z_\mathrm{R}, z_\mathrm{T}) \approx \frac{je^{-j\pi/4 + jk_1X + j\phi_D(t_s)}}{2\sqrt{2\pi k_1 X}} \times \left[1 + \frac{\varepsilon}{8k_0}\left(\frac{X}{2h - z_\mathrm{T} - z_\mathrm{R}}\right)^3 e^{\frac{2jk_1(h - z_\mathrm{T})(h - z_\mathrm{R})}{X}}\right]. \quad (30)$$

Then, the second term of (30) represents the field reflected by an interface defined at $z = h$, which equals the duct height. In addition, the field magnitude corresponds to the broadening of the bundle of the rays.

In (27), if $\nu_+ - \nu_- + \xi s_0 = 0$, $p_0 = -(\nu_+ - \nu_- + \xi s_0)/2 = 0$ and then the denominator vanishes and then, $|g_R(X; z_\mathrm{R}, z_\mathrm{T})|$ goes to infinity, which has no physical meaning. From (C6), this corresponds to $p_0 = 0 \Rightarrow t_0 = 0$. Then from (C1), $\xi = \sqrt{\nu_+} + \sqrt{\nu_-}$, and the corresponding abscissa is

$$X_2 = 2\left(\sqrt{\frac{h - z_\mathrm{T}}{\varepsilon}} + \sqrt{\frac{h - z_\mathrm{R}}{\varepsilon}}\right). \quad (31)$$

For example, for $h = 20$ m, $z_\mathrm{T} = 10$ m, $z_\mathrm{R} = 0$ and $\varepsilon = 0.0001\ \mathrm{m}^{-1}$, we have $X_2 \approx 1527$ m $< X_1$. As shown in the next subsection, the region defined for $X > X_2$ corresponds to the shadow zone for the **direct** field (g_D).

The unphysical behavior of the **reflected** field (g_R) comes from the fact that expansion (20) used for $\mathcal{R}$ is not valid as $t \to 0^-$ ($t = -p^2$). Indeed, as $t \to 0^-$, $|\mathcal{R}| \to \infty$. For $t = 0$, without expansion, $\mathcal{R} = e^{j\pi/3}$. Thus, to avoid the divergence of $|\mathcal{R}|$, in (27) from (20), $p_0^3 = (-t_0)^{3/2}$ is substituted for $1/|8\mathcal{R}(t_0)| = 1/|8\mathcal{R}(-p_0^2)|$, in which $\mathcal{R}$ is computed without approximation. With this substitution, near $\xi = \sqrt{\nu_+} + \sqrt{\nu_-}$ ($p_0 \to 0$ or $\nu_+ - \nu_- + \xi s_0 \to 0$), the reflected field behaves as $\sqrt{\nu_+ - \nu_- + \xi s_0}$ and then vanishes. This means that the reflected field does not exist in the shadow zone defined as $\xi > \sqrt{\nu_+} + \sqrt{\nu_-}$.

b) Shadow region for the direct field g_D: Appendix B summarizes the works of [8] (chapter 7) and [9] (appendix A) to derive analytically the integration of integral (18) over t. Then, from (B8) and (B14), we have

$$g_D(X; z_\mathrm{R}, z_\mathrm{T}) \approx \frac{je^{-j\pi/4 + jk_0X}}{2\sqrt{2\pi k_1 X}}\left[e^{j\phi_D(t_s)}\frac{1 - s_{\xi_0}}{2} + \sqrt{\frac{\xi}{\alpha_0}}e^{j\phi(\alpha_0)}f(s_{\xi_0}\mu\xi_0)s_{\xi_0} + \Phi_{D,3}\right]. \quad (32)$$

where the functions $\phi(\alpha)$ and f are expressed from (B2) and (B6), respectively, and

$$\begin{cases} \alpha_0 = \sqrt{\nu_+} + \sqrt{\nu_-} \\ \xi_0 = \xi - \alpha_0 \\ \alpha_0 = \sqrt{\nu_+} + \sqrt{\nu_-} = \left(\frac{k_0}{\varepsilon}\right)^{\frac{1}{3}}(\tau_\mathrm{T} + \tau_\mathrm{R}) \\ \mu^2 = -\partial_\alpha^2\phi/2 = \sqrt{\frac{\nu_+\nu_-}{\nu_+ + \nu_-}} \\ \sqrt{\frac{\xi}{\alpha_0}} = \sqrt{\frac{\varepsilon X}{2(\tau_\mathrm{T} + \tau_\mathrm{R})}} \\ \mu\xi_0 = \sqrt{\frac{k_1}{\varepsilon}}\sqrt{\frac{\tau_\mathrm{T}\tau_\mathrm{R}}{\tau_\mathrm{T} + \tau_\mathrm{R}}}(\varepsilon X/2 - \tau_\mathrm{T} - \tau_\mathrm{R}) \\ \phi(\alpha_0) = \frac{2}{3}\left(\nu_+^{\frac{3}{2}} + \nu_-^{\frac{3}{2}}\right) = \frac{2k_0}{3\varepsilon}\left(\tau_\mathrm{T}^3 + \tau_\mathrm{R}^3\right) \end{cases} \quad (33)$$

$\tau_\mathrm{R} = \sqrt{\varepsilon(h - z_\mathrm{R})} \geq 0$ and $\tau_\mathrm{T} = \sqrt{\varepsilon(h - z_\mathrm{T})} \geq 0$. In addition,

$$\begin{aligned} \Phi_{D,3} &\approx \frac{e^{-j\sqrt{\sigma}\delta}}{\sqrt{2}} f^*\left(\sqrt{\sigma\xi} + \frac{\delta}{2\sqrt{\xi}}\right) \\ &\approx e^{-\frac{jk_0}{\varepsilon}\left|\tau_\mathrm{R}^2 - \tau_\mathrm{T}^2\right|\sqrt{\tau_\mathrm{R}^2 + \tau_\mathrm{T}^2}} \\ &\quad \times f^*\left(\sqrt{\frac{k_0X\left(\tau_\mathrm{R}^2 + \tau_\mathrm{T}^2\right)}{2}}\left[1 + \frac{\left|\tau_\mathrm{R}^2 - \tau_\mathrm{T}^2\right|}{\varepsilon X\sqrt{\tau_\mathrm{R}^2 + \tau_\mathrm{T}^2}}\right]\right) \end{aligned} \quad (34)$$

where the symbol * stands for the complex conjugate.

In (32), $\xi_0 < 0$ ($s_{\xi_0} = \mathrm{sgn}(\xi_0) = -1$) corresponds to the illuminated region whereas $\xi_0 \geq 0$ ($s_{\xi_0} = \mathrm{sgn}(\xi_0) = +1$) corresponds to the shadow region. For $\xi_0 = 0$, $\xi = \alpha_0$, $\phi(\xi) = \phi(\alpha_0) = \phi_D(t_s)$, $\varepsilon X = 2(\tau_\mathrm{T} + \tau_\mathrm{R})$, $f(0) = 1/2$ and $\sqrt{\xi/\alpha_0} = 1$. Then, (32) is continuous for $\xi_0 = 0$.

In the illuminated region $\xi_0 < 0$, if $\varepsilon X \ll 2(\tau_\mathrm{T} + \tau_\mathrm{R})$ ($\xi \ll \alpha_0$) and $-\mu\xi_0 \gg 1$, then $\sqrt{\xi/\alpha_0} \ll 1$ and $|f(-\mu\xi_0)| \ll 1$ and the second term of (32) can be neglected. Neglecting ϕ_{D3} (numerically, we will show that its contribution is minor) and comparing then the resulting equation with (15) obtained under the PWE, the same equation is found with $R \approx X$ ($|z_\mathrm{R} - z_\mathrm{T}| \ll X$).

2) Green Function for $z_\mathrm{R} \geq h$: Receiver Outside the Duct: For $z_\mathrm{R} \geq h$ (case 3 of Fig. 1), the spectral Green function is expressed from (12). Using the same way as in the previous subsection, the Transmitted spatial Green function is expressed as

$$g_T(X; z_\mathrm{R}, z_\mathrm{T}) \approx \frac{e^{jk_1X}}{4\pi Hk_1}\int_C \frac{w_1(t_\mathrm{T})e^{j\sqrt{-t}(z_\mathrm{R} - h)/H}}{w_1'(t) - j\sqrt{-t}w_1(t)}e^{j\xi t}dt. \quad (35)$$

For the illuminated zone, $t \ll 0$ and $t_\mathrm{T} = t - \nu_\mathrm{T} \ll 0$ ($\nu_\mathrm{T} = (h - z_\mathrm{T})/H \geq 0$), which is equivalent to apply the WKB approximation. Then, from (A1) and (A2), we have

$$\begin{cases} w_1(t_\mathrm{T}) \approx e^{\frac{j\pi}{4}}(\nu_\mathrm{T} - t)^{-1/4}e^{\frac{2j}{3}(\nu_\mathrm{T} - t)^{\frac{3}{2}}} \\ w_1'(t) - j\sqrt{-t}w_1(t) \approx -2je^{\frac{j\pi}{4}}(-t)^{\frac{1}{4}}e^{\frac{2j}{3}(-t)^{\frac{3}{2}}} \end{cases} \quad (36)$$

leading from (35) to

$$g_T(X; z_\mathrm{R}, z_\mathrm{T}) \approx \frac{je^{jk_1X}}{8\pi Hk_1}\int_C \frac{e^{j\phi_T(t)}}{[(-t)(\nu_\mathrm{T} - t)]^{\frac{1}{4}}}dt \quad (37)$$

where

$$\phi_T(t) = \xi t + \frac{2}{3}(\nu_\mathrm{T} - t)^{\frac{3}{2}} - \frac{2}{3}(-t)^{\frac{3}{2}} - \nu_\mathrm{R}\sqrt{-t} \quad (38)$$

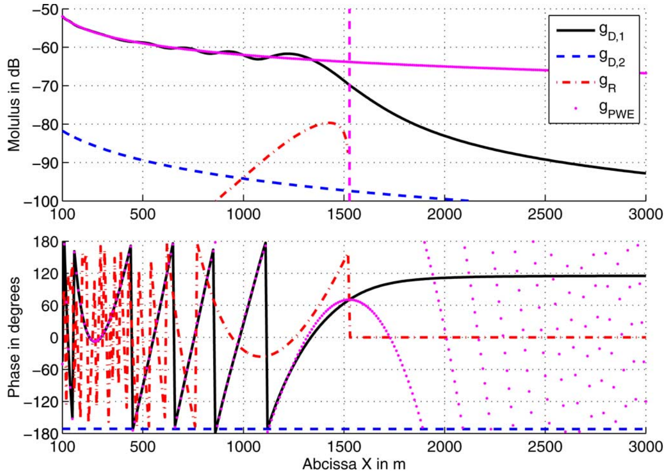

Fig. 3. Green functions $g_{D,1}$ (Eq. (32)), $g_{D,2}$ (Eq. (32)), g_R (Eq. (27)) and $g_{\rm PWE}$ (Eq. (15)) versus the horizontal distance $X = x_{\rm R} - x_{\rm T}$ in m and for a receiver height $z_{\rm R} = 0$. Top: Modulus. Bottom: Phase. The parameters are $x_{\rm T} = 0$ (transmitter abscissa), $z_{\rm T} = 10$ m (transmitter height), $\varepsilon = 10^{-4}$ m^{-1} (duct parameter), $h = 20$ m (duct height) and $\lambda_0 = 0.1$ m (wavelength). The vertical dashed line indicates the separation between the illuminated and the shadow regions.

and $\nu_{\rm R} = (h - z_{\rm R})/H \leq 0$. In Appendix D, we show that

$$g_T(X; z_{\rm R}, z_{\rm T}) \approx \frac{je^{-j\pi/4 + jk_1X}}{2\sqrt{2\pi k_1 X}} \left(\frac{\xi^2}{4\left[\phi''_T(t_0)\right]^2 p_0^2 \left(\nu_{\rm T} + p_0^2\right)} \right)^{\frac{1}{4}} \times e^{j\phi_T(t_0) + j\left\{\mathrm{sgn}\left[\phi''_T(t_0)\right]+1\right\}\pi/4} \quad (39)$$

where $t_0 = -p_0^2$ and $p_0 = s_0 - a_2/3$, in which s_0 and a_2 are expressed from (D6) and (D3), respectively. In addition, ϕ''_T is expressed from (D1).

3) Numerical Results: Fig. 3 plots Green functions $g_{D,1}$, $g_{D,2}$, g_R and $g_{\rm PWE}$ versus the horizontal distance $X = x_{\rm R} - x_{\rm T}$ in m and for a receiver height $z_{\rm R} = 0$. Top: Modulus. Bottom: Phase. The parameters are $x_{\rm T} = 0$ (transmitter abscissa), $z_{\rm T} = 10$ m (transmitter height), $\varepsilon = 10^{-4}$ m^{-1} (duct parameter), $h = 20$ m (duct height) and $\lambda_0 = 0.1$ m (wavelength). The vertical dashed line indicates the separation between the illuminated and the shadow regions. The labels in the legend means that:

- $g_{D,1}$ is computed from the first two terms of (32),
- $g_{D,2}$ is computed from the last term of (32) (related to $\Phi_{D,3}$),
- g_R is computed from (27),
- g_{PWE} is the spatial Green function obtained under the PWE approximation and computed from (15).

In the illuminated zone (on the left of the vertical dashed line), Fig. 3 shows that g_{PWE} and $g_{D,1}$ give similar results and that $g_{D,1}$ has an oscillatory behavior because it is defined as the sum of two terms, leading to an interference phenomenon. In the shadow region, g_{PWE} slowly decreases, whereas $g_{D,1}$ rapidly decreases. As expected, the PWE approximation is not valid in this region. Fig. 3 also shows that the contributions of $g_{D,2}$ and g_R are minor in comparison to $g_{D,1}$, leading to the conclusion that the total spatial Green function $g \approx g_{D,1}$. In addition, g_R contributes only in the illuminated region, first increases when X increases and then strongly decreases near the limit of the illuminated zone.

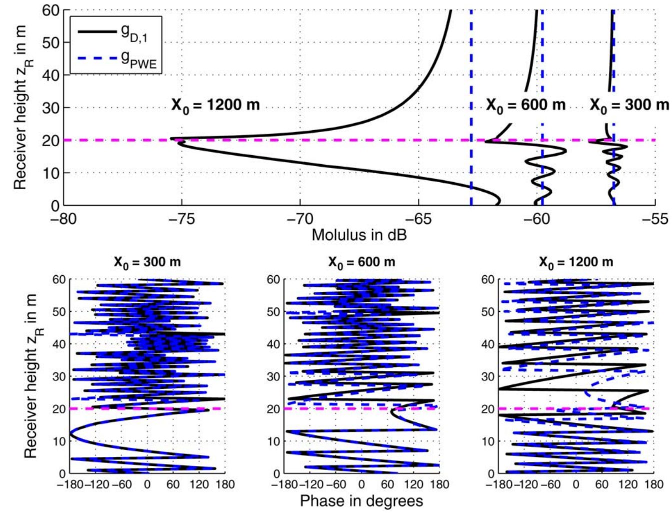

Fig. 4. Receiver height $z_{\rm R}$ in m versus the Green functions $g_{D,1}$ and $g_{\rm PWE}$ for horizontal distances $X = X_0 = \{300, 600, 1200\}$ m. Top: Modulus. Bottom: Phase. The parameters are the same as in Fig. 3.

Fig. 4 plots the receiver height $z_{\rm R}$ in m versus the Green functions $g_{D,1}$ and $g_{\rm PWE}$ for horizontal distances $X = X_0 = \{300, 600, 1200\}$ m. Top: Modulus. Bottom: Phase. The parameters are the same as in Fig. 3. For a given X_0, $|g_{\rm PWE}|$ is constant whereas $|g_{D,1}|$ has an oscillatory behavior around a mean value close to $|g_{\rm PWE}|$. In addition, as X_0 increases (or approaches the shadow zone), the oscillation number increases and the difference between $|g_{D,1}|$ and $|g_{\rm PWE}|$ increases. For $z_{\rm R} = h$, the continuity of the Green function is ensured and then, the use of approximations to calculate analytically the Green function did not modify the boundary conditions at $z_{\rm R} = h$ (see also Fig. 6).

C. Green Function for $z_{\rm T} \geq h$: Transmitter Outside the Duct

1) Green Function for $z_{\rm R} < h$: Receiver Inside the Duct: For $z_{\rm R} < h$ (case 2 of Fig. 1), the spectral Green function is expressed from (9). For $(z_{\rm R} \geq h, z_{\rm T} < h)$, (12) is the same as (9) obtained for $(z_{\rm R} < h, z_{\rm T} \geq h)$ by substituting $z_{\rm R}$ for $z_{\rm T}$. Thus, the spatial Green function is

$$\begin{aligned} g_T(X; z_{\rm R}, z_{\rm T}) &= \text{Eq. (25)}|_{(z_{\rm T}, z_{\rm R}) \to (z_{\rm R}, z_{\rm T})} \\ &\approx \text{Eq. (39)}|_{(z_{\rm T}, z_{\rm R}) \to (z_{\rm R}, z_{\rm T})}. \end{aligned} \quad (40)$$

2) Green Function for $z_{\rm R} \geq h$: Receiver Outside the Duct: For $t \ll 0$, in (7), $(1-\alpha)/(1+\alpha) \to 0$, which means that the reflection coefficient vanishes. Indeed, since $n(h^+) = n(h^-)$, the use of the WKB approximation implies a zero reflection coefficient. Then, from (9) and since $t = -H^2 k_{1z}^2$, we have

$$g_D(X; z_{\rm R}, z_{\rm T}) \approx \frac{jH}{4\pi} \int_C \frac{e^{j\sqrt{-t}|z_{\rm T} - z_{\rm R}|/H}}{\sqrt{-t}} e^{j\xi t} dt. \quad (41)$$

Thus, From (24), we show that

$$g_D(X; z_{\rm R}, z_{\rm T}) \approx \frac{je^{-j\pi/4 + jk_1X}}{2\sqrt{2\pi k_1 X}} \times e^{\frac{jk_1(z_{\rm T} - z_{\rm R})^2}{2X}}. \quad (42)$$

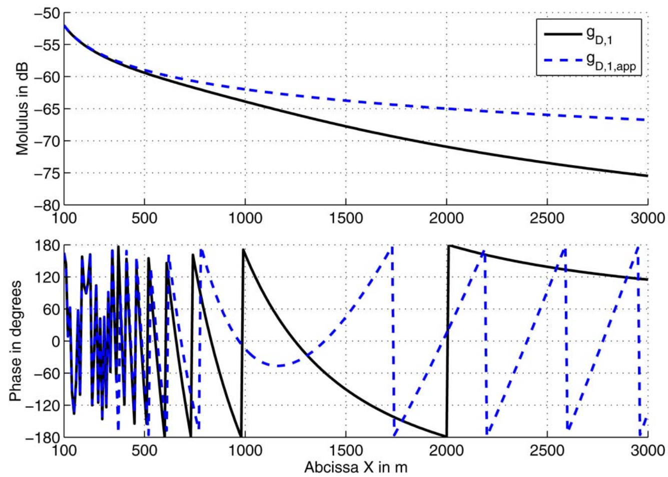

Fig. 5. Same variations as in Fig. 3, but for $z_{\mathrm{T}} = 30\ \mathrm{m}$.

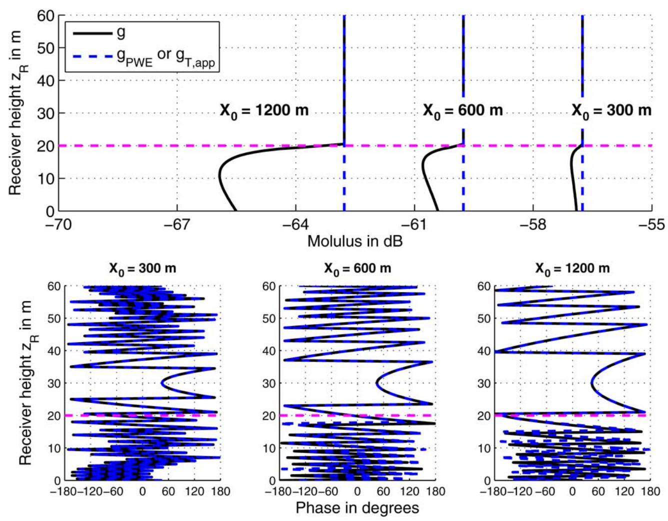

Fig. 6. Same variations as in Fig. 4, but for $z_{\mathrm{T}} = 30\ \mathrm{m}$.

The Green function is equal to the Green function expressed from the PWE (15), in which the radial distance $R \approx X + (z_{\mathrm{R}} - z_{\mathrm{T}})^2/(2X)$ in the phase term and $\varepsilon = 0$.

3) Numerical Results: Fig. 5 plots the same variations as in Fig. 3, but for $z_{\mathrm{T}} = 30\ \mathrm{m}$ (transmitter outside the duct).

Since $z_{\mathrm{R}} = 0 < h$, the Green function is expressed from g_T (40). In addition, $g_{T,\mathrm{app}}$ is plotted and it is derived from g_T as $\varepsilon \to 0$. Its expression is

$$g_{T,\mathrm{app}}(X; z_{\mathrm{R}}, z_{\mathrm{T}}) \approx \frac{je^{-j\pi/4 + jk_1 X + \frac{jk_1 (z_{\mathrm{T}} - z_{\mathrm{R}})^2}{2X}}}{2\sqrt{2\pi k_1 X}} \times \frac{e^{\frac{jk_1 \epsilon X (h - z_{\mathrm{R}})^2}{4(z_{\mathrm{T}} - z_{\mathrm{R}})}}}{1 - \frac{\varepsilon (h - z_{\mathrm{R}})(3h - z_{\mathrm{R}} - 2z_{\mathrm{T}}) X^2}{2(z_{\mathrm{T}} - z_{\mathrm{R}})^3}} + \mathcal{O}(\varepsilon^2). \quad (43)$$

In (43), the first term is related to the propagation in free space ($\varepsilon = 0$) under the PWE approximation and the second term is related to the duct effect, which modifies both the phase and the amplitude of the field. Fig. 5 shows that the series expansion (43) is valid only for X close to zero. In addition, no shadow zone occurs.

Fig. 6 plots the same variations as in Fig. 4, but for $z_{\mathrm{T}} = 30\ \mathrm{m}$. For $z_{\mathrm{R}} \geq h$, the Green function equals Green function computed from PWE (see (42)). For $z_{\mathrm{R}} < h$, g_T differs from $g_{T,\mathrm{app}}$ because $g_{T,\mathrm{app}}$ is valid only for X_0 close to zero (see Fig. 5).

Numerical results, not depicted here, showed that the spatial Green function satisfies the reciprocity principle.

IV. Conclusion

For a two-dimensional problem, this paper presents the evaluation of the spatial Green function of a space made up of homogeneous medium overlying a duct with a linear-square refractive index profile. From the boundary conditions, the exact spectral Green function is derived with the help of the Airy functions. To have a closed-form expression of the corresponding spatial Green function, the method of SD (Steepest Descents) is applied and comparisons are made with the PWE.

When the transmitter is located inside the duct (often met for practical applications), for abscissa near the transmitter, the results are the same as those obtained from the PWE. On the other hand, far from the transmitter, the spatial Green function rapidly decreases in the shadow zone, whereas the PWE results slowly decrease. This means that the PWE is not valid in this region. In addition, we show that the contribution of the "Reflected" Green function (27) and that computed from (32) are negligible in comparison to the "Direct" (32) Green function.

In a future paper, by adding a rough surface of profile $\zeta(x)$ (centered on $z = 0$), the Green function above the rough surface will be computed by solving the integral equations, which requires the Green function derived in this paper. When the PWE is used as a propagator, the currents computed on the rough surface are also approximated. On the contrary, by solving rigorously the integral equations, no approximation is used to calculate the propagator and the currents on the rough surface. Thus, the use of the spatial Green function evaluated in this paper and combined with the BIE will allow us to have a benchmark method and then to test the accuracy of the PWE.

Appendix A
Expansion of the Airy Functions

For $t \to -\infty$, with $w = (2/3)(-t)^{3/2} > 0$, the Airy functions and their derivatives can be expanded as [6] (chapter 3, pages 181–186), [10] (chapter 10, starting from page 446)

$$\begin{cases} v(t) = (-t)^{-1/4} \left[\sin v - \frac{a_1}{w} \cos v + \mathcal{O}\left(\frac{1}{w^2}\right)\right] \\ u(t) = (-t)^{-1/4} \left[\cos v + \frac{a_1}{w} \sin v + \mathcal{O}\left(\frac{1}{w^2}\right)\right] \end{cases} \quad (A1)$$

and

$$\begin{cases} \partial_t v(t) = (-t)^{\frac{1}{4}} \left[-\cos v + \frac{b_1}{w} \sin v + \mathcal{O}\left(\frac{1}{w^2}\right)\right] \\ \partial_t u(t) = (-t)^{\frac{1}{4}} \left[\sin v + \frac{b_1}{w} \cos v + \mathcal{O}\left(\frac{1}{w^2}\right)\right] \end{cases} \quad (A2)$$

where $v = w + \pi/4$, $a_1 = 5/72$, and $b_1 = 7/72$.

Appendix B
Evaluation of Integral (18)

From [8], integral (18) can be written as $\Phi_D = \Phi_{D,1} + \Phi_{D,2}$ where $\Phi_{D,2} \approx e^{j\phi(t_s)}$ obtained from a conventional SD technique based on (24), where $\phi(t_s)$ is expressed from (26). $\Phi_{D,2}$ corresponds then to the field in the illuminated zone. For the evaluation of $\Phi_{D,1}$, using their integral representation for both factors $w_1(t-\nu_-)$ and $w_1(t-\nu_+)$ and performing the integration over t, a double contour integral is obtained, in which new variables can be introduced to perform one integration. The resulting equation is then [8]

$$\Phi_{D,1} = \frac{\sqrt{\xi}}{2\pi j} \int_{\Gamma_1} \frac{e^{j\phi(\alpha)} d\alpha}{\sqrt{\alpha}(\alpha - \xi)} \tag{B1}$$

where the contour $\Gamma_1 =]+j\infty; \xi^+] \cup]\xi^+; +\infty e^{-j\pi/6}[$, in which the superscript $^+$ means from the *right* $(\alpha - \xi > 0)$. In addition

$$\phi(\alpha) = -\frac{\alpha^3}{12} + \frac{\alpha(\nu_+ + \nu_-)}{2} + \frac{(\nu_+ - \nu_-)^2}{4\alpha}. \tag{B2}$$

The residue of integral (B1) at the point $\alpha = \xi$ equals the quantity $\Phi_{D,2}$. Thus [8]

$$\Phi_D = \Phi_{D,1} + \Phi_{D,2} = \frac{\sqrt{\xi}}{2\pi j} \int_{\Gamma_1'} \frac{e^{j\phi(\alpha)} d\alpha}{\sqrt{\alpha}(\alpha - \xi)} \tag{B3}$$

where $\Gamma_1' =] + j\infty; \xi^-] \cup]\xi^-; +\infty e^{-j\pi/6}[$ (the value ξ is included in Γ_1'), in which the superscript $^-$ means from the *left* ($\alpha - \xi$ can be either negative or positive).

To evaluate (B3), the method of SD is applied. The saddle points of ϕ, defined as $\partial_\alpha \phi = 0$ are $\pm(\sqrt{\nu_-} \pm \sqrt{\nu_+})$. For $\xi \geq 0$, the saddle points which contribute are $\alpha_0 = \sqrt{\nu_-} + \sqrt{\nu_+} > 0$ and $\alpha_1 = |\sqrt{\nu_-} - \sqrt{\nu_+}| \geq 0$ because they can be close to the poles $(0, \xi)$ of the integrand (B3). In the textbook of Fock [8], the contribution of the saddle point $\alpha_1 = |\sqrt{\nu_-} - \sqrt{\nu_+}|$ close to zero is not considered since is not encircled in the contour Γ_1 (or Γ_1'). On the other hand, Kukushkin [9] derived this contribution and then the contour Γ_1 is substituted for $\Gamma_1 =] + j\infty; 0[\cup]0; \xi^+] \cup]\xi^+; +\infty e^{-j\pi/6}[$.

A. Saddle Point $\alpha_0 = \nu_+ + \nu_-$

For α_0, the variable $\xi_0 = \xi - \alpha_0$ is introduced, and the contour Γ_{10} equals to Γ_1 or Γ_1', is defined but cutting the horizontal axis at the point $\xi = \alpha_0$. If $\xi_0 \leq 0$, then the contour Γ_{10} is equal to Γ_1 and the resulting integral is $\Phi_{D,1}$. If $\xi_0 > 0$, then the contour Γ_{10} is similar to Γ_1' and the resulting integral is $\Phi_D = \Phi_{D,1} + \Phi_{D,2}$. To calculate the contribution of the saddle point α_0 with $\Gamma_1' = \Gamma_{10}$, we assume for $\alpha \to \alpha_0$ that $\phi(\alpha) \approx \phi(\alpha_0) - \mu^2(\alpha - \alpha_0)^2$ and $1/\sqrt{\alpha} \approx 1/\sqrt{\alpha_0}$ in (B3), where

$$\begin{cases} \mu^2 = -\phi''(\alpha_0)/2 = \frac{\sqrt{\nu_+ \nu_-}}{\sqrt{\nu_+} + \sqrt{\nu_-}} > 0 \\ \phi(\alpha_0) = \frac{2}{3}\left(\nu_+^{\frac{3}{2}} + \nu_-^{\frac{3}{2}}\right) \end{cases}. \tag{B4}$$

In (B1), the contour is then deformed as $\alpha = \alpha_0 + pe^{-j\pi/4}$ ($(\alpha - \alpha_0)^2 = -jp^2$ and then $-j\mu^2(\alpha - \alpha_0)^2 = -\mu^2 p^2 \leq 0$) with $p \in \mathbb{R}$). Then [8]

$$\frac{\sqrt{\xi}}{2\pi j} \int_{\Gamma_{10}} \frac{e^{j\phi(\alpha)} d\alpha}{\sqrt{\alpha}(\alpha - \xi)} \approx \sqrt{\frac{\xi}{\alpha_0}} e^{j\phi(\alpha_0)} f(s_{\xi_0} \mu \xi_0) s_{\xi_0} \tag{B5}$$

with [10]

$$\begin{aligned} f(\alpha) &= \frac{e^{-j\alpha^2 - j\pi/4}}{\sqrt{\pi}} \int_\alpha^\infty e^{ju^2} du \\ &= \frac{e^{-j\alpha^2 - j\pi/4}}{\sqrt{2}} \left\{ \left[\frac{1}{2} - \mathrm{C}_1(\alpha)\right] + j\left[\frac{1}{2} - \mathrm{S}_1(\alpha)\right] \right\} \\ &= \frac{e^{-j\alpha^2}}{2} \mathrm{erfc}(e^{-j\pi/4}\alpha) \end{aligned} \tag{B6}$$

and

$$f(\alpha) = \frac{j}{2\sqrt{\pi}\alpha} + \frac{1}{4\sqrt{\pi}\alpha^3} + \mathrm{o}\left(\frac{1}{\alpha^3}\right) \alpha \gg 1. \tag{B7}$$

In addition, $s_{\xi_0} = \mathrm{sgn}(\xi_0)$, $\mathrm{C}_1(\alpha) + j\mathrm{S}_1(\alpha) = \sqrt{2/\pi} \int_0^\alpha e^{jt^2} dt$, in which C_1 and S_1 are the Fresnel integrals and erf is the error function defined as $\mathrm{erf}(\alpha) = \sqrt{2/\pi} \int_0^\alpha e^{-t^2} dt$ and $\mathrm{erfc} = 1 - \mathrm{erf}$.

In conclusion, for $\xi_0 > 0$, (B5) gives Φ_D whereas for $\xi_0 \leq 0$, (B5) gives $\Phi_{D,1} = \Phi_D - \Phi_{D,2}$. Then

$$\Phi_D \approx e^{j\phi(\alpha_0)} \frac{1 - s_{\xi_0}}{2} + \sqrt{\frac{\xi}{\alpha_0}} e^{j\phi(\alpha_0)} \times f(s_{\xi_0} \mu \xi_0) s_{\xi_0}. \tag{B8}$$

B. Saddle Point $\alpha_1 = |\nu_+ - \nu_-|$

The integral $\Phi_{D,1}$ (B1) must be evaluated when the saddle point $\alpha_1 = |\nu_+ - \nu_-|$ is close to zero. The same way is used as in [9], in which the misprints are corrected in this appendix.

Since α is close to zero, we have from (B1)

$$\begin{aligned} \Phi_1 &= \frac{\sqrt{\xi}}{2\pi j} \int_0^\infty \frac{e^{-\frac{j\alpha^3}{12} + j\alpha\sigma + \frac{j\delta^2}{4\alpha}}}{\sqrt{\alpha}(\alpha - \xi)} d\alpha \\ &= \frac{\sqrt{\xi}}{2\pi j} \int_0^\infty \frac{e^{j\alpha\sigma + \frac{j\delta^2}{4\alpha}}}{\sqrt{\alpha}(\alpha - \xi)} \sum_{n=0}^\infty \left(\frac{\alpha^3}{n!12j}\right)^n d\alpha \\ &\approx \frac{\sqrt{\xi}}{2\pi j} \left[\Psi(\sigma, \delta, \xi) + \frac{1}{12} \frac{\partial^3 \Psi}{\partial \sigma^3} + \ldots\right] \end{aligned} \tag{B9}$$

where

$$\Psi = e^{j\sigma\xi} \Psi_1, \quad \Psi_1 = \int_0^\infty \frac{e^{j(\alpha - \xi)\sigma + \frac{j\delta^2}{4\alpha}}}{\sqrt{\alpha}(\alpha - \xi)} d\alpha \tag{B10}$$

and $\sigma = \nu_+ + \nu_-$ and $\delta = |\nu_+ - \nu_-| = \alpha_1$.

To derive the function Ψ_1, the function $\Psi_2 = -je^{j\sigma\xi} \partial \Psi_1 / \partial \sigma$ is introduced and defined by

$$\Psi_2 = \int_0^\infty \frac{e^{j\alpha\sigma + \frac{j\delta^2}{4\alpha}}}{\sqrt{\alpha}} d\alpha = -e^{j\pi/4 - j\delta\sqrt{\sigma}} \sqrt{\frac{\pi}{\sigma}}. \tag{B11}$$

Then, the function Ψ_1 is derived from integrating Ψ_2 over σ, leading to

$$\Psi_1(\sigma,\delta,\xi) = \frac{\pi}{j\sqrt{\xi}} e^{\frac{j\delta^2}{4\xi}} \operatorname{erf}\left[e^{\frac{j\pi}{4}}\left(\sqrt{\sigma\xi}+\frac{\delta}{2\sqrt{\xi}}\right)\right] + C(\delta,\xi) \tag{B12}$$

where the function C depends only on the variables (δ,ξ). This function is then calculated from (B10) by taking $\sigma = 0$, leading to $C(\delta,\xi) = j\pi/\sqrt{\xi}e^{j\delta^2/(4\xi)}$. Then, from (B10) and (B12), we obtain

$$\Psi(\sigma,\delta,\xi) = \frac{j\pi}{\sqrt{\xi}} e^{\frac{j\delta^2}{4\xi}+j\sigma\xi} \operatorname{erfc}\left[e^{\frac{j\pi}{4}}\left(\sqrt{\sigma\xi}+\frac{\delta}{2\sqrt{\xi}}\right)\right]. \tag{B13}$$

Reporting (B13) into (B9), we obtain

$$\begin{aligned}\Phi_{D,3} &\approx \frac{e^{-j\sqrt{\sigma}\delta+j\xi_1^2}}{2}\operatorname{erfc}\left(e^{\frac{j\pi}{4}}\xi_1\right)\\ &\approx \frac{e^{-j\sqrt{\sigma}\delta}}{\sqrt{2}} f^*(\xi_1)\end{aligned} \tag{B14}$$

where $\xi_1 = \sqrt{\sigma\xi} + \delta/(2\sqrt{\xi})$ (real number) and the symbol * stands for the complex conjugate. In addition, calculating $\partial^3\Psi/\partial\sigma^3$ analytically, we can show numerically that $|\partial^3\Psi/\partial\sigma^3| \ll 12|\Psi|$.

Appendix C
Evaluation of Integral (19) in the Illuminated Region

In this appendix, integral (19) is evaluated from (24) and from the works of [8] (chapter 12).

From (23), we have

$$\begin{cases}\phi'_R(t) = \xi - \sqrt{\nu_- - t} - \sqrt{\nu_+ - t} + 2\sqrt{-t}\\ \phi''_R(t) = \frac{1}{2\sqrt{\nu_- - t}} + \frac{1}{2\sqrt{\nu_+ - t}} - \frac{1}{\sqrt{-t}}\end{cases}. \tag{C1}$$

With $t = -p^2 > 0$, the root of $\phi'_R(p_0) = 0$ satisfies then

$$\sqrt{\nu_- + p_0^2} + \sqrt{\nu_+ + p_0^2} = 2p_0 + \xi. \tag{C2}$$

In addition, we have

$$\begin{cases}\sqrt{\nu_- + p_0^2} - p_0 = \frac{1}{2}\left(\xi + \frac{\nu_- - \nu_+}{2p_0+\xi}\right)\\ \sqrt{\nu_+ + p_0^2} - p_0 = \frac{1}{2}\left(\xi - \frac{\nu_- - \nu_+}{2p_0+\xi}\right)\end{cases}. \tag{C3}$$

Isolating p_0 for each subequation of (C3) and equating them, $s_0 = \nu_- - \nu_+/2p_0 + \xi \leq 0$ satisfies the following cubic equation

$$s_0^3 - s_0(\xi^2 + 2\nu_+ + 2\nu_-) + 2\xi(\nu_- - \nu_+) = 0. \tag{C4}$$

Then, the physical solution (real solution) is

$$s_0 = 2\mu\sin\left(\frac{\alpha}{3}\right) \quad \text{with} \quad \begin{cases}\mu^2 = \frac{1}{3}(\xi^2 + 2\nu_+ + 2\nu_-)\\ \sin\alpha = \frac{\xi(\nu_- - \nu_+)}{\mu^3} \leq 0\end{cases}. \tag{C5}$$

The root p_0 is then obtained from s_0 as

$$p_0 = \frac{1}{2}\left(\frac{\nu_- - \nu_+}{s_0} - \xi\right). \tag{C6}$$

Reporting (C6) and (C3) into (23) and (C1), we show

$$\begin{cases}\phi_R(s_0) = \frac{(\nu_- - \nu_+)s_0}{3} - \frac{\xi^3}{12} + \frac{(\nu_- - \nu_+)(2\nu_+ + 2\nu_- + \xi^2)}{6s_0}\\ \qquad - \frac{\xi(\nu_- - \nu_+)}{12s_0^3}\\ \phi''_R(s_0) \leq 0\\ \left\{\left[(\nu_+ - t)(\nu_- - t)\right]^{\frac{1}{4}}(-t)^{\frac{3}{2}}\right\}^2 \times \phi''_R(t)|_{t=t_0} =\\ \qquad -\frac{(\nu_+ - \nu_-)\xi + s_0^3}{2(\nu_+ - \nu_- + \xi s_0)} \times p_0^3\end{cases}. \tag{C7}$$

The substitution of (C7) into (22) and the use of (24) leads to (27).

Appendix D
Evaluation of Integral (37)

In this appendix, integral (37) is evaluated from (24). From (38), we have

$$\begin{cases}\phi'_T(t) = \xi - \sqrt{\nu_{\rm T} - t} + \sqrt{-t} + \frac{\nu_{\rm R}}{2\sqrt{-t}}\\ \phi''_T(t) = \frac{1}{2\sqrt{\nu_{\rm T} - t}} - \frac{1}{2\sqrt{-t}} + \frac{\nu_{\rm R}}{4(-t)^{\frac{3}{2}}}\end{cases}. \tag{D1}$$

The root of $\phi'_T(p_0) = 0$ satisfies then

$$p_0^3 + a_2p_0^2 + a_1p_0 + a_0 = 0 \tag{D2}$$

where

$$a_2 = \frac{\xi^2 + \nu_{\rm R} - \nu_{\rm T}}{2\xi}, \quad a_1 = \frac{\nu_{\rm R}}{2}, \quad a_0 = \frac{\nu_{\rm R}^2}{8\xi} \tag{D3}$$

and the condition $2p_0\xi + 2p_0^2 + \nu_{\rm R} = 2p_0\sqrt{p_0^2 + \nu_{\rm T}} \geq 0$.

Letting $s_0 = p_0 + a_2/3$, we have then

$$s_0^3 - 3s_0p_1 + 2q_1 = 0 \tag{D4}$$

where

$$p_1 = \frac{a_2^2}{9} - \frac{a_1}{3}, \quad q_1 = \frac{a_2^3}{27} - \frac{a_1a_2}{6} + \frac{a_0}{2}. \tag{D5}$$

The physical solution is then ($p_0 \geq 0$ and $2p_0\xi + 2p_0^2 - \nu_{\rm R} \geq 0$)

$$s_0 = \sqrt{p_1}\left[\sqrt{3}\cos\left(\frac{\alpha}{3}\right) - \sin\left(\frac{\alpha}{3}\right)\right] \tag{D6}$$

where

$$\sin\alpha = \frac{q_1}{p_1\sqrt{p_1}}. \tag{D7}$$

References

[1] M. Levy, *Parabolic Equation Methods for Electromagnetic Wave Propagation*, ser. Electromagnetic Waves 45. London: Inst. Elect. Eng., 2000.

[2] B. J. Uscinski, "Sound propagation with a linear sound-speed profile over a rough surface," *J. Acoust. Soc. Am.*, vol. 94, no. 1, pp. 491–498, 1993.

[3] R. S. Awadallah, "Rough Surface Scattering and Propagation Over Rough Terrain in Ducting Environments," Ph.D. dissertation, Virginia Polytech. Inst. State Univ., Blacksburg, VA, USA, 1998.

[4] R.-S. Awadallah and G. S. Brown, "Low-grazing angle scattering from rough surfaces in a duct formed by a linear-square refractive index profile," *IEEE Trans. Antennas Propag.*, vol. 48, no. 5, pp. 1461–1474, 2000.

[5] A. J. Robins, "Exact solutions of the Helmholtz equation for plane wave propagation in a medium variable density and sound speed," *J. Acoust. Soc. Am.*, vol. 93, no. 3, pp. 1347–1352, 1993.

[6] L. M. Brekhovskikh, *Waves in Layered Media*, 2nd ed. New York, NY, USA: Academic Press, 1980.

[7] L. B. Felsen and N. Marcuvitz, *Radiation and Scattering Waves*. Englewood Cliffs, NJ, USA: Prentice-Hall, 1973.

[8] V. A. Fock, *Electromagnetic Diffraction and Propagation Problems*. Paris: Pergamon Press, 1965.

[9] A. Kukushkin, *Radio Wave Propagation in the Marine Boundary Layer*. London: Wiley-VCH, 2004.

[10] M. Abramowitz and I. A. Stegun, *Handbook of Mathematical Functions*. Mineola, NY, USA: Dover Publications, 1972.

[11] T. Ishihara and L. B. Felsen, "Hybrid ray-mode parameterization of high frequency propagation in an open waveguide with inhomogeneous transverse refractive index: Formulation and application to a bilinear surface duct," *IEEE Trans. Antennas Propag.*, vol. 39, no. 6, pp. 780–788, 1991.

[12] T. Ishihara and L. B. Felsen, "Hybrid ray-mode parameterization of high frequency propagation in an open waveguide with inhomogeneous transverse refractive index: Numerical results and quality assessment," *IEEE Trans. Antennas Propag.*, vol. 39, no. 6, pp. 789–797, 1991.

Christophe Bourlier was born in La Flèche, France on July 6, 1971. He received the M.S. degree in electronics from the University of Rennes (France), in 1995 and the Ph.D. degree from the SEI (Système Électronique et Informatique) Laboratory, in 1999.

While at the the University of Rennes, he was with the Laboratory of Radiocommunication where he worked on antennas coupling in the VHF-HF band. Currently, he is with the IETR Laboratory (Institut d'Electronique et des Télécommunications de Rennes, France) at Polytech Nantes (University of Nantes, France). He works as a Researcher at the National Center for Scientific Research on electromagnetic wave scattering from rough surfaces and objects for remote sensing applications and Radar signatures. He is the author of more than 130 journal articles and conference papers.

Nicolas Pinel was born in Saint-Brieuc, France, in 1980. He received the Engineering degree and M.S. degree in electronics and electrical engineering both from Polytech Nantes (Ecole polytechnique de l'université de Nantes), Nantes, France, in 2003 and the Ph.D. degree from the University of Nantes, France, in 2006.

He is currently working as a Research Engineer in the IETR Laboratory (Institut d'Électronique et de Télécommunications de Rennes), Nantes, France. His research interests are in the areas of radar and optical remote sensing, scattering and propagation. In particular, he works on asymptotic methods of electromagnetic wave scattering from random rough surfaces and layers.